

Structural and magnetic properties of Mg-substituted Co ferrite nanopowders

LEZHONG LI*, XIAOXI ZHONG RUI WANG XIAOQIANG TU, LEI HE

College of Optoelectronic Technology, Chengdu University of Information Technology, Chengdu 610225, People's Republic of China

Mg-substituted Co ferrite nanopowders, $Mg_xCo_{1-x}Fe_2O_4$ ($0 \leq x \leq 1.0$), were synthesized by sol-gel auto-combustion method. The effects of Mg substitution on the structural and magnetic properties have been investigated. The DTA and TG results indicated that there were three steps of combustion process. X-ray diffraction and vibrating scanning magnetometer were used to characterize the structural and magnetic properties. XRD revealed single-phase of cubic spinel. And the X-ray diffraction patterns showed that the lattice parameter, average crystallite size and X-ray density decreased with the increase of Mg substitution. The saturation magnetization, magnetocrystalline anisotropy constant and coercivity decreased with the increase of Mg substitution.

(Received March 28, 2017; accepted April 5, 2018)

Keywords: Co ferrite nanopowder, Sol-gel auto-combustion process, Mg substitution, Structure, Magnetic properties

1. Introduction

The unique properties of ferrite nanopowders have generated more interest in the science community because high surface to volume ratio resulting in novel phenomena's of nanomagnetism such as superparamagnetism, magnetic quantum tunneling and spin-glasslike behavior etc. [1].

It is well known that the ferrites $MeFe_2O_4$ with the spinel structure are based on a face-center cubic lattice of the oxygen ions. Each spinel unit cell contains eight formula units. In each unit cell, there are 64 tetrahedral sites (A sites) and 32 octahedral sites (B sites). Therefore, the chemical, structural, and magnetic properties of ferrite are strongly influenced by their composition and microstructure, which are sensitive to the preparation methodologies [2]. They show various magnetic properties depending on the cation distribution. Various cations can be placed in the structure of AB_2O_4 in A site and B site to tune its magnetic properties. Magnetic properties of spinel ferrites can be varied systematically by changing the identity of the divalent cations without changing the spinel crystal structure [3]. There is a very interesting result that $MgFe_2O_4$ shows magnetism, although Mg^{2+} ion is non-magnetic. The main reason is due to the incomplete inverse spinel structure of $MgFe_2O_4$ [4, 5], which indicates that it is possible Mg^{2+} ions occupy A and B sites, and Mg^{2+} ions can be affected the properties of spinel ferrite nanopowders.

For Co bulk ferrite, Ahmed et al. [6] had mainly

studied the the dependence of the molar magnetic susceptibility on absolute temperature as a function of magnetic field intensity for Mg-substituted Co bulk ferrite. Nlebedim et al. [7] had studied the effect of changing the concentration of Mg, substituted for Fe, on the structural, magnetic, and magnetostrictive properties of Co ferrite. In theory, Hamedoun [8] had studied magnetic properties of magnetic $Co_{1-x}Mg_xFe_2O_4$ spinel by HTSE method. However, in the work reported to date, aiming at the properites of Co bulk ferrites with different Mg substitution prepared by the standard ceramic technique, there are seldom investigation about the Mg-substituted Co ferrite nanopowders synthesized by sol-gel auto-combustion method.

In the present work, Mg-substituted Co ferrite nanopowders were prepared by sol-gel auto-combustion method because it has advantages of being able to use inexpensive precursors, a simple preparation method and low sintering temperature that results in well dispersed homogenous, nano-sized and highly reactive ferrite powder [9, 10]. Accordingly, the effects of Mg substitution on the structural and magnetic properties in Co ferrite nanopowders are investigated.

2. Experimental procedures

The samples of $Mg_xCo_{1-x}Fe_2O_4$ ($x=0, 0.20, 0.40, 0.60, 0.80, 1.0$) ferrite nanopowders were synthesized by sol-gel auto-combustion method. Stoichiometric quantities of

analytical grade $\text{Fe}(\text{NO}_3)_3 \cdot 9\text{H}_2\text{O}$, $\text{Co}(\text{NO}_3)_2 \cdot 6\text{H}_2\text{O}$ and $\text{Mg}(\text{NO}_3)_2 \cdot 4\text{H}_2\text{O}$ were first dissolved in deionized water and stirred for 15 minutes. After the nitrates completely dissolved, the citric acid was added to the resulting solution and the molar ratio of citric acid and metal nitrates was taken as 3:1. Then, the prepared solution was continuously stirred for 3 hours at 80°C to form the gel precursors. To maintain the pH value at 7 an aqueous ammonia solution was added drop-wise after the gel precursors cooled to room temperature. The gel solution was dried at 85°C until a dry gel precursor was obtained. Finally, the dried gel was ignited in self-propagation combustion to obtain ferrite powders.

Simultaneous differential thermal analysis-thermogravimetry (DTA–TG) measurements were carried out on as-prepared precursors, up to 800°C at a heating rate of $10^\circ\text{C}/\text{min}$, using Shimadzu DTG-60 thermal analyzer. The phase identification of the prepared nanopowders was performed by DX 2700 X-ray diffractometer (XRD) (Cu target, $K\alpha$ radiation, the wavelength is 0.154056 nm , 35 kV , 25 mA) at room temperature. The static magnetic properties measured by the VSM-220 vibrating sample magnetometer (VSM) at room temperature.

3. Results and discussion

3.1. Thermal decomposition of the as-prepared precursor

The minimum temperature for the complete decomposition process, which can be considered as the minimum temperature for the calcination process, can be estimated from the thermal behavior measurements of the dried precursors [11]. Fig. 1 shows typical DTA-TG curves in air for the as-prepared gel precursor with $\text{Mg}_{0.6}\text{Co}_{0.4}\text{Fe}_{2.0}\text{O}_4$. The DTA and TG results indicate that there are three steps of combustion process. The first step occurs before 200°C which can be attributed to the evaporation of the residual water. The weight change is approximately 12.3%. The endothermic DTA peak at about 133°C is attributed to the dehydration of the precursor. The second step occurs at about 221°C which associated with a relatively sharp and intense exothermic peak. The weight change is approximately 77.4%. It indicates that the decomposition of the gel occurs suddenly in a single step, as observed in other systems [11, 12]. The third step occurs in the range 290°C to 425°C are attributed to the oxidative decomposition of the residual nitrate and organic matter. The weight change is approximately 4.5%. The weight of the precursor appears to be constant for temperatures above 425°C .

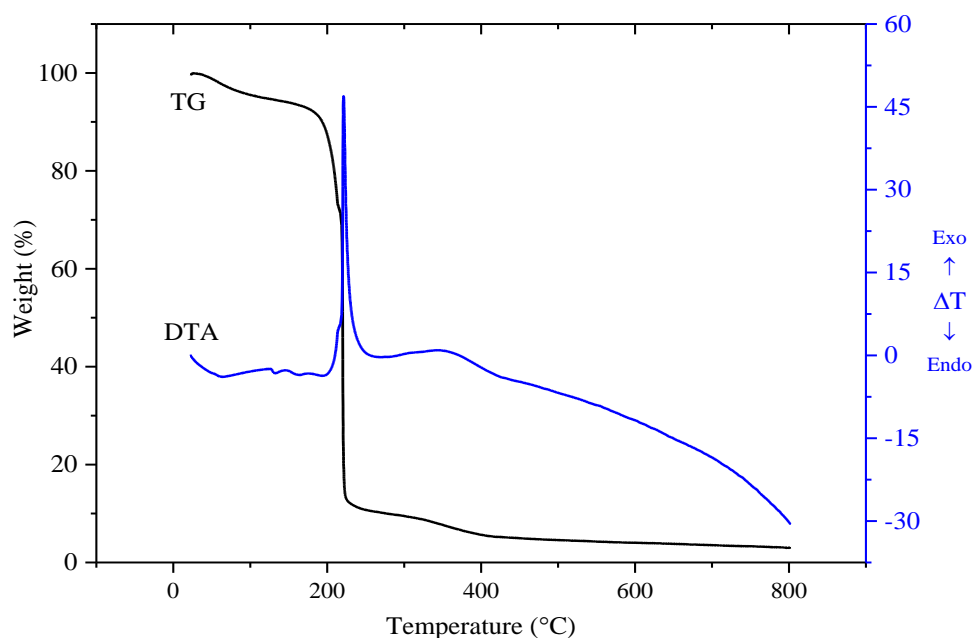


Fig. 1. DTA-TG curves in air of as-prepared precursors of $\text{Mg}_{0.6}\text{Co}_{0.4}\text{Fe}_{2.0}\text{O}_4$

3.2. Structural properties

X-ray diffraction patterns of $\text{Mg}_x\text{Co}_{1-x}\text{Fe}_2\text{O}_4$ ferrite nanopowders are shown in Fig. 2. The patterns indicate that all samples match well with the characteristic of cubic spinel structure and without unidentified extra peaks in the

range of measurement precision. The lattice parameter (a) and average crystallite size (D) of all samples are calculated according to XRD data and the results are shown in Table 1. The lattice parameter and average particle size decrease from 0.8409 nm to 0.8398 nm and 28.0 nm to 21.3 nm , respectively.

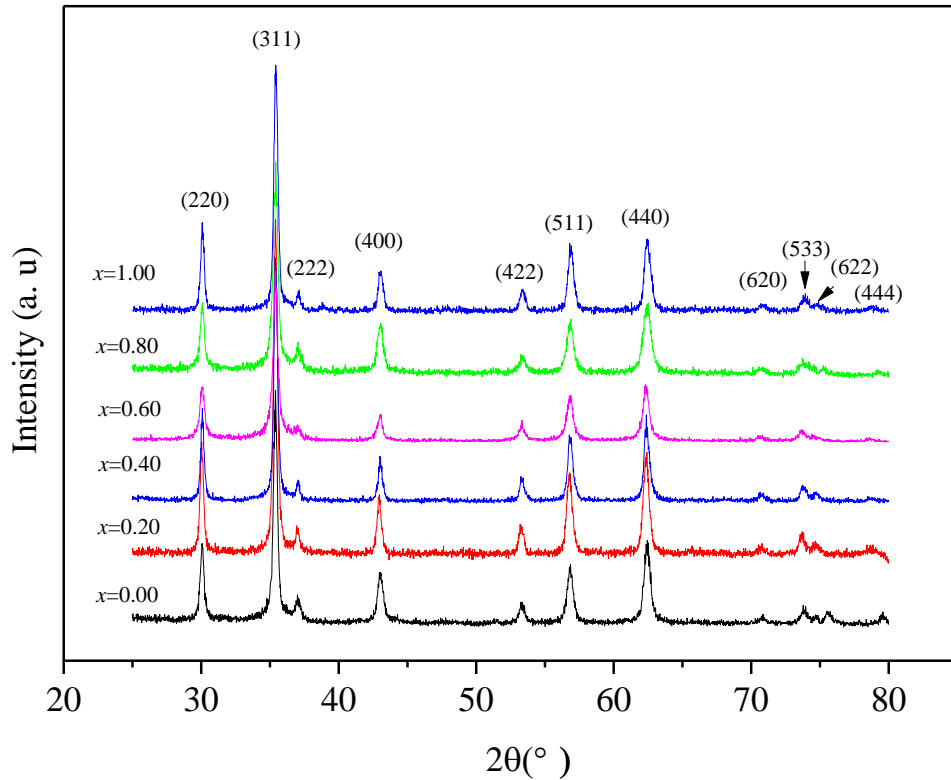


Fig. 2. X-ray diffraction patterns of $Mg_xCo_{1-x}Fe_2O_4$ ferrite nanopowders

The lattice parameter (a) of the samples can be calculated using the following relation [13]:

$$a = d_{hkl} \sqrt{h^2 + k^2 + l^2} \quad (1)$$

where $(h \ k \ l)$ are the Miller indices and d_{hkl} is the inter-planar spacing. The average crystallite size is calculated according to Debye-Scherrer equation [13-15]:

$$D = \frac{0.9\lambda}{\beta \cos \theta} \quad (2)$$

where λ is wavelength of the X-ray radiation, β is measure of broadening of diffraction due to size effect and θ is the Bragg's angle. The X-ray density (d_x) is calculated using the following relation [16,17]:

$$d_x = \frac{8M_w}{N_A a^3} \quad (3)$$

where M_w is the molecular weight; N_A is the Avogadro's parameter and a is the lattice parameter.

From Table 1 it is clear that, the lattice parameter (a), average crystallite size calculated by Debye-Scherrer's equation, and the X-ray density (d_x) decrease with the increase of Mg substitution. The slightly decrease of lattice parameter with Mg substitution increasing could be explained as follows. In ferrites, Mg^{2+} ion has a stronger preference for the B-sites than Co^{2+} [7]. Therefore, nonmagnetic Mg substitutes into the B-sites for magnetic Co. And according to the ionic radii, Mg^{2+} ion (0.072 nm) is smaller than that of the Co^{2+} ion (0.0745 nm), then the lattice parameter decreases with Mg substitution. The average crystallite size decreases with the increase of Mg substitution maybe due to the generated Mg oxide during the auto-combustion process acts as a microstructural stabilizer responsible for finer crystallite size [18]. The decrease in the density mainly due to the decrease in mass overcomes the decrease in volume of the unit cell. Consequently, the substitution of Co^{2+} ions of higher atomic weight (58.93) with lower atomic weight Mg^{2+} ions (24.31) results in the decrease of density from 5.244 to 4.488 g/cm³.

Table 1. Lattice parameter (a), crystallite size (D) and X-ray density (d_x) of $Mg_xCo_{1-x}Fe_2O_4$ ferrite nanopowders

x	0	0.20	0.40	0.60	0.80	1.0
a (nm)	0.8409	0.8407	0.8403	0.8402	0.8400	0.8398
D (nm)	28.0	27.1	26.5	22.9	22.3	21.3
d_x (g/cm ³)	5.244	5.093	4.945	4.791	4.640	4.488

3.3. Magnetic properties

Fig. 3 shows the hysteresis loops of $Mg_xCo_{1-x}Fe_2O_4$ ferrite nanopowders. The saturation magnetization (M_s), magnetocrystalline anisotropy constant (K_1) and coercivity (H_c) of nanopowders as a function of Mg substitution (x) are shown in Fig. 4. The saturation magnetization (M_s), magnetocrystalline anisotropy constant (K_1) and coercivity (H_c) decrease with the increase of Mg substitution.

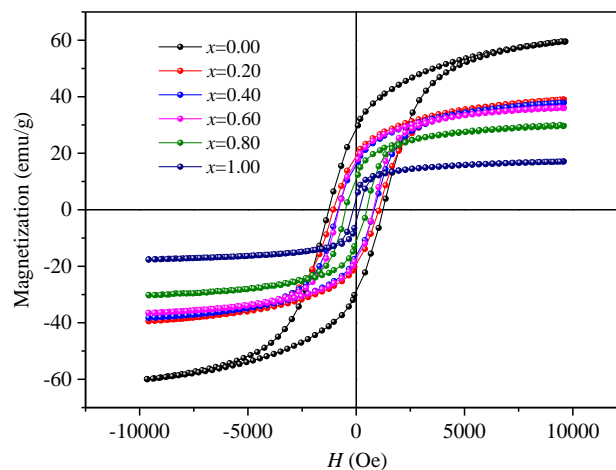


Fig. 3. Hysteresis loops of $Mg_xCo_{1-x}Fe_2O_4$ ferrite nanopowders

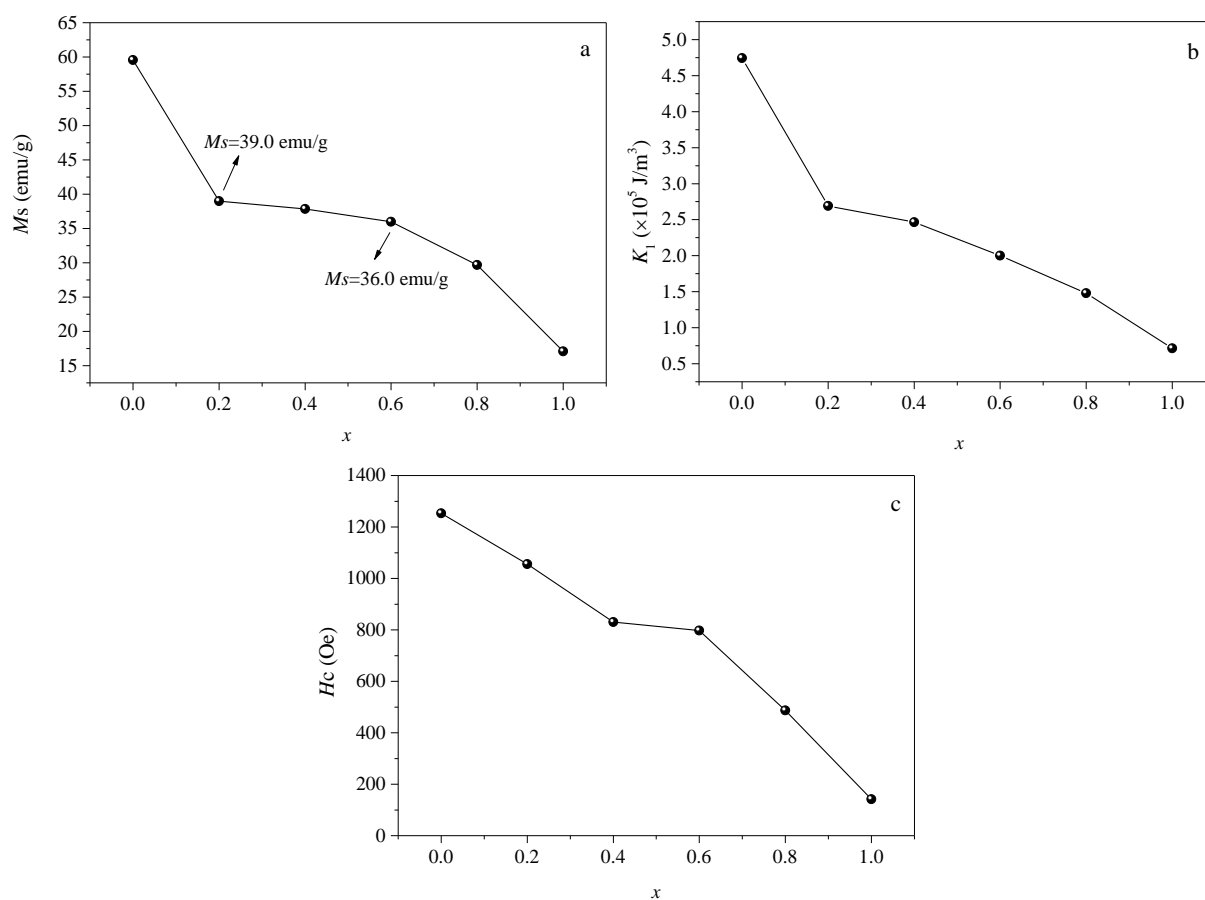


Fig. 4. M_s (a), K_1 (b) and H_c (c) of $Mg_xCo_{1-x}Fe_2O_4$ ferrite nanopowders

Magnetic properties of ferrites are sensitively dependent on the structure, composition, defects, crystallite size, internal strain and cation distribution. According to site preference of ions [7, 25], the cations distribution of nanopowders can be written as $(\text{Fe})_A[\text{Mg}_x\text{Co}_{1-x}\text{Fe}]_B\text{O}_4$. And based on Néel's two sublattice model of ferrimagnetisms, the magnetic moment in Bohr magneton of $\text{Mg}_x\text{Co}_{1-x}\text{Fe}_2\text{O}_4$ ferrite nanopowders can be calculated by the following equation:

$$M_{AB} = |M_B - M_A| = |3 - 3x|\mu_B \quad (4)$$

where M_A and M_B are the magnetic moments in the A and B sites, and the magnetic moments of Mg^{2+} , Co^{2+} , and Fe^{3+} ions are 0, 3, and 5 μ_B , respectively. Simultaneously, the term of saturation magnetization (M_s) is defined as the vector sum of magnetic moment per unit cell, and can be written as the following equation:

$$M_s = \frac{8M_{AB}}{a^3} \quad (5)$$

Thus, according to equations (4) and (5), and the little variations of lattices parameters (a) with Mg substitution, M_s decreases with the increase of Mg substitution. It is worth noting there is a little decrease from 39.0 to 36.0 emu/g of M_s when $0.2 \leq x \leq 0.6$. The cations distribution in MgFe_2O_4 indicated that this ferrite is 86% inverted as given by neutrons scattering [20]. Therefore, partial nonmagnetic Mg^{2+} ions enter into tetrahedral site of the present system when $x \geq 0.2$ results in the little variation of M_s when $0.2 \leq x \leq 0.6$. Spinel ferrite consist of intersublattice (A-B) super-exchange interactions and intra-sub-lattice (A-A) and (B-B) exchange interactions. Inter-sub-lattice superexchange interactions of the cations on the (A-B) are much stronger than the (A-A) and (B-B) intra-sub-lattice exchange interactions [21]. So, excessive nonmagnetic cations in tetrahedral site will decrease the magnetic ions pair with octahedral sites which would result in the decrease of A-B superexchange interaction. Consequently, M_s sharply decreases with the increase of Mg substitution when $x > 0.60$.

The first cubic anisotropy coefficient (K_1) of the samples, obtaining by the Law of Approach to saturation magnetization as equations (6) and (7) [22], is shown in Fig. 4 (b).

$$M = M_s \left(1 - \frac{a}{H} - \frac{b}{H^2} - \dots \right) + \kappa H \quad (6)$$

$$b = \frac{8}{105} \frac{K_1^2}{\mu_0^2 M_s^2} \quad (7)$$

where M_s and H are the saturation magnetization and applied field respectively. The coefficients a and b are related to the stress and crystal anisotropy of the sample respectively. κH is the forced magnetization term. The numerical coefficient 8/105 is for random polycrystalline

specimens with cubic anisotropy, μ_0 is the permeability of free space. The variation of the estimated magnetocrystalline anisotropy constant (K_1) with different Mg substitution is shown in Fig. 4(b). It indicates that K_1 decreases with the increase of Mg substitution which mainly due to the Mg^{2+} ion is nonmagnetic ion. With the increase of nonmagnetic Mg ions substituted for magnetic Co ions in the ferrite nanopowders, the magnetocrystalline anisotropy field decreases. Eventually, K_1 decreases with the increase of Mg substitution.

The coercivity (H_c) of ferrite nanopowders as a function of Mg substitution (x) is shown in Fig. 4(c), which indicates that H_c monotonically decreases with the increase of Mg substitution. This results mainly due to the nonmagnetic ions enter the lattices results in the decrease of magnetocrystalline anisotropy energy which can be confirmed by the increase of the K_1 (Fig. 4(b)). In addition, according to the Stoner-Wohlfarth single domain theory [23], H_c decreases with the decrease of crystallite size when the crystallite is single domain structure. So, from Table 1 and Fig. 4(c), the crystallite with single domain structure may be another possible reason for the decrease of H_c .

4. Conclusions

Mg-substituted Co ferrite nanopowders, $\text{Mg}_x\text{Co}_{1-x}\text{Fe}_2\text{O}_4$ ($0 \leq x \leq 1.0$), have been synthesized by sol-gel auto-combustion method. The structural and static magnetic properties of nanopowders have been investigated. The DTA and TG results indicated that there were three steps of combustion process. The X-ray diffraction patterns showed that the lattice parameter and average particle size decreased from 0.8409 nm to 0.8398 nm and 28.0 nm to 21.3 nm, respectively. The saturation magnetization (M_s), magnetocrystalline anisotropy constant (K_1) and coercivity (H_c) decreased with the increase of Mg substitution.

Acknowledgments

This work was supported by the National Natural Science Foundation of China under Grant no. 51502025.

References

- [1] M. S. Khandekar, R. C. Kambale, J. Y. Patil, Y. D. Kolekar, S. S. Suryavanshi, J. Alloys Compd. **509**, 1861 (2011).
- [2] F. Li, J. J. Liu, D. G. Evans, X. Duan, Chem. Mater. **16**, 1597 (2004).
- [3] X. M. Liu, G. Yang, S. Y. Fu, Mater. Sci. Eng. C **27**, 750 (2007).
- [4] Y. Ichiyanagi, M. Kubota, S. Moritake, Y. Kanazawa,

- T. Yamada, T. Uehashi, *J. Magn. Magn. Mater.* **310**, 2378 (2007).
- [5] M. Raghasudha, D. Ravinder, P. Veerasomaiah, *J. Magn. Magn. Mater.* **355**, 210 (2014).
- [6] M. A. Ahmed, A. A. El-Khawlani, *J. Magn. Magn. Mater.* **321**, 1959 (2009).
- [7] I. C. Nlebedim, R. L. Hadimani, R. Prozorov, D. C. Jiles, *J. App. Phys.* **113**, 17A928 (2013).
- [8] M. Hamedoun, A. Benyoussef, M. Bousmina, *Physica B* **406**, 1633 (2011).
- [9] J. Y. Patil, M. S. Khandekar, I. S. Mulla, S. S. Suryavanshi, *Curr. Appl. Phys.* **12**, 319 (2012).
- [10] N. Dhananjaya, H. Nagabhushana, B. M. Nagabhushana, B. Rudraswamy, C. Shivakumara, R. P. S. Chakradhar, *J. Alloys Compd.* **509**, 2368 (2011).
- [11] W. A. Bayoumy, M. A. Gabal, *J. Alloys Compd.* **506**, 205 (2010).
- [12] M. A. Gabal, Y. M. A. Angari, *Mater. Chem. Phys.* **118**, 153 (2009).
- [13] B. D. Cullity, *Elements of X-ray Diffraction*, Addison Wesley Publishing: Massachusetts, 1959.
- [14] M. H. Mahmoud, C. M. Williams, J. Cai, I. Siu, J. C. Walker, *J. Magn. Magn. Mater.* **261**, 314 (2003).
- [15] M. H. Ibrahim, M. S. Seehra, G. Srinivasan, *J. App. Phys.* **75**, 6822 (1994).
- [16] S. Amiri, H. Shokrollahi, *J. Magn. Magn. Mater.* **345**, 18 (2013).
- [17] E. R. Kumar, R. Jayaprakash, S. Kumar, *Mater. Sci. Semicond. Process* **17**, 173 (2014).
- [18] E. Rezlescu, N. Rezlescu, P.D. Popa, L. Rezlescu, C. Pasnicu, M. L. Craus, *Mater. Res. Bull.* **33**, 915 (1998).
- [19] A. Miller, *J. Appl. Phys.* **30**, S24 (1959).
- [20] N. S. Murthy, L. M. Rao, R. J. Begum, M. G. Natera, S. I. Youssef, *J. Phys. Colloq.* **32**, 318 (1971).
- [21] V. Chaudhari, S. E. Shirsath, M. L. Mane, *Crystallographic, J. Alloys Compd.* **549**, 213 (2013)
- [22] W. D. Zhong, *Ferromagnetism*, Science Press, Beijing, 1998.
- [23] E. C. Stoner, E. P. Wohlfarth, *IEEE Trans. Magn.* **27**, 3475 (1991).

*Corresponding author: lezhong_li@163.com